Annals of Mathematical Sciences and Applications
Volume 2, Number 2, 319–340, 2017

Weighted essentially non-oscillatory schemes for Degasperis-Procesi equation with discontinuous solutions

Yinhua Xia* and Yan Xu†

In this paper, we develop the high order weighted essentially non-oscillatory (WENO) schemes for solving the Degasperis-Procesi (DP) equation, including finite volume (FV) and finite difference (FD) methods. The DP equation contains nonlinear high order derivatives, and possibly discontinuous or sharp transition solutions. The finite volume method is designed based on the total variation bounded property of the DP equation. And the finite difference method is constructed based on the L^2 stability of the DP equation. Due to the adoption of the WENO reconstruction, both schemes are arbitrary high order accuracy and shock capturing. The numerical simulation results for different types of solutions of the nonlinear Degasperis-Procesi equation are provided to illustrate the accuracy and capability of the methods.

AMS 2000 subject classifications: Primary 65M06, 65M08; secondary 35Q53.
Keywords and phrases: Degasperis-Procesi equation, discontinuous solution, weighted essentially non-oscillatory schemes, finite difference method, finite volume method.

1. Introduction

In this paper, we consider weighted essentially non-oscillatory (WENO) schemes for the Degasperis-Procesi (DP) equation

$$u_t - u_{txx} + 4f(u)_x = f(u)_{xxx}, \tag{1.1}$$

for a real function $u(x,t)$ of the two variables x and t, where $f(u) = u^2/2$. We develop finite volume WENO and finite difference WENO methods. Due to the adoption of the WENO reconstruction, both schemes are high order accuracy and shock capturing.

*Research supported by NSFC grant No. 11371342, No. 11471306.
†Research supported by NSFC grant No. 11371342, No. 11526212.

Degasperis-Procesi equation is a real nonlinear partial differential equation (PDE) which models propagation of nonlinear dispersive waves and is solvable by the methods of soliton theory. Degasperis and Procesi [7] studied the following family of third order dispersive PDE conservation laws,

$$u_t + c_0 u_x + \kappa u_{xxx} - \epsilon^2 u_{txx} = (c_1 u^2 + c_2 u_x^2 + c_3 u u_{xx})_x, \tag{1.2}$$

where κ, ϵ, c_0, c_1, c_2, and c_3 are real constants. They found that there are only three equations that satisfy the asymptotic integrability condition within this family, namely, the KdV equation ($\epsilon = c_2 = c_3 = 0$), the Camassa-Holm (CH) equation ($c_1 = -\frac{3c_3}{2\epsilon^2}$, $c_2 = \frac{c_3}{2}$) and one new equation ($c_1 = -\frac{2c_3}{2\epsilon^2}$, $c_2 = c_3$, the DP equation). The DP equation is very special because it belongs to the class of integrable equations, that are PDEs with infinitely many conservation laws. This PDE is not only of mathematical interest but it has also proved to be an approximate model of shallow water wave propagation in the small amplitude and long wavelength regime [15, 9, 6, 13].

One of the important features of the DP equation is that it has not only peaked solutions [8], for example, $u(x,t) = ce^{-|x-ct|}$, but also shock waves to the equation [18, 3], for example

$$u(x,t) = -\frac{1}{t+c}\text{sign}(x)e^{-|x|}, \quad c > 0. \tag{1.3}$$

Three useful conservation laws for the DP equation are:

$$E_1(u) = \int_R (u - u_{xx})dx,\ E_2(u) = \int_R (u - u_{xx})v dx,\ E_3(u) = \int_R u^3 dx,$$

where $4v - v_{xx} = u$. The conservation laws $E_i(u)$ can not guarantee the boundedness of the slope of a wave in the L^2-norm. There is no way to find conservation laws controlling the H^1-norm. Such nonlinearly dispersive partial differential equations support peakon solutions and shock solutions. The lack of smoothness of the solution introduces more difficulty in the numerical computation. It is a challenge to design stable and high order accurate numerical schemes for solving this equation. In this paper, we develop the finite volume and the finite difference methods for the DP equation by adopting the WENO reconstruction. Comparing with the existing numerical methods, the FV/FD WENO methods are also high order accurate for smooth solutions but no limiter or post-processing procedure is needed for discontinuous solutions.

There are many analytical and numerical works for the DP equations in recent years. Coclite and Karlsen proved existence and uniqueness results for

entropy weak solutions belonging to the class $L^1 \cap BV$ in [3] and uniqueness result for entropy weak solutions by replacing the Kružzkov-type entropy inequalities by an Oleinik-type estimate in [4]. Coclite, Karlsen and Risebro [5] constructed several operator splitting schemes and proved that solutions of these finite difference schemes converge to entropy weak solutions. Moreover, they provided several numerical examples to show that shock solutions can form independently of the smoothness of the initial data. Another operator splitting method was proposed for the DP equation in [10], which is based on the second-order TVD scheme and linearized implicit finite difference method. Miyatake and Matsuo [19] proposed two conservative finite difference schemes to preserve two invariants E_2 and E_3 for the DP equation. And compact finite difference scheme has been used by Yu et al. [27] with symplectic implicit Runge-Kutta time integration. Fourier spectral methods with the Gegenbauer post-processing were developed for the discontinuous solutions in [24]. The geometric numerical integration was also considered in [2]. In [12], a particle method based on the multi-shock peakon solutions was investigated for entropy weak solutions of the DP equation numerically. Local discontinuous Galerkin (LDG) and direct DG finite element methods have been designed for the DP equation by Xu and Shu [26] and Liu et al. [16], after developing the LDG methods for the CH equation [25].

The weighted essentially non-oscillatory (WENO) finite difference and finite volume schemes are high order numerical methods for problems with piecewise smooth solutions containing discontinuities. The WENO schemes [17, 14] were based on the earlier work of essentially non-oscillatory (ENO) schemes [11, 20]. The key idea lies at the approximation level, where a nonlinear adaptive procedure is used to automatically choose the locally smoothest stencil, hence avoiding crossing discontinuities in the interpolation procedure as much as possible. WENO schemes are available for arbitrarily high order accuracy [1]. WENO schemes have been quite successful in applications, especially for problems containing both shocks and complicated smooth solution structures, such as compressible turbulence simulations and aeroacoustics. We refer to the review papers [22, 23] for the development and application of WENO schemes.

The remains of this paper is organized as follows. In section 2 we develop the finite volume WENO scheme for the DP equation, based on the total variation bounded property. In section 3, we first design the linear finite difference method and prove the L^2 stability. Then we construct the finite difference WENO scheme based on the L^2 stable linear scheme. Section 4 contains the numerical tests to demonstrate the accuracy and capability of the methods. Concluding remarks are given in Section 5.

2. Finite volume method

In this section, we develop the finite volume method for the DP equation based on the total variation bounded property.

Consider the DP equation (1.1) with the initial condition $u(x,0)=u_0(x)$ in the interval $[-L,L]$, and assume the solution satisfies the periodic boundary condition. By introducing the auxiliary variable m, the DP equation can also be written in the following hyperbolic-elliptic system

$$\begin{cases} u_t + f(u)_x + p = 0, \\ m - p_x = 0, \\ p - m_x = 3f(u)_x. \end{cases} \tag{2.1}$$

Given a grid

$$-L = x_{\frac{1}{2}} < x_{\frac{3}{2}} < \cdots < x_{N-\frac{1}{2}} < x_{N+\frac{1}{2}} = L,$$

we define the cells, cell centers and cell sizes by

$$I_i = [x_{i-\frac{1}{2}}, x_{i+\frac{1}{2}}],\ x_i = \frac{1}{2}(x_{i-\frac{1}{2}} + x_{i+\frac{1}{2}}),\ h_i = x_{i+\frac{1}{2}} - x_{i-\frac{1}{2}},\ i = 1, \cdots, N.$$

For the finite volume schemes, or schemes based on cell averages, we solve the integrated version of the DP equation. We integrate (2.1) over the interval I_i to obtain

$$\begin{cases} \frac{\bar{u}(x_i,t)}{dt} + \frac{1}{h_i}\left(f(u(x_{i+\frac{1}{2}})) - f(u(x_{i-\frac{1}{2}}))\right) + \bar{p}(x_i,t) = 0, \\ \bar{m}(x_i,t) - \frac{1}{h_i}\left(p(x_{i+\frac{1}{2}}) - p(x_{i-\frac{1}{2}})\right) = 0, \\ \bar{p}(x_i,t) - \frac{1}{h_i}\left(m(x_{i+\frac{1}{2}}) - m(x_{i-\frac{1}{2}})\right) = \frac{3}{h_i}\left(f(u(x_{i+\frac{1}{2}})) - f(u(x_{i-\frac{1}{2}}))\right), \end{cases} \tag{2.2}$$

where

$$\bar{u}(x_i,t) = \frac{1}{h_i}\int_{I_i} u(x,t)dx$$

is the cell average, similar to $\bar{m}(x_i,t)$ and $\bar{p}(x_i,t)$. We approximate (2.2) by the following conservation scheme

$$
\begin{cases}
\frac{\bar{u}_i(t)}{dt} + \frac{1}{h_i}\left(\hat{f}_{i+\frac{1}{2}} - \hat{f}_{i-\frac{1}{2}}\right) + \bar{p}_i = 0, \\
\bar{m}_i(t) - \frac{1}{h_i}\left(\hat{p}_{i+\frac{1}{2}} - \hat{p}_{i-\frac{1}{2}}\right) = 0, \\
\bar{p}_i(t) - \frac{1}{h_i}\left(\hat{m}_{i+\frac{1}{2}} - \hat{m}_{i-\frac{1}{2}}\right) = \frac{3}{h_i}\left(\hat{f}_{i+\frac{1}{2}} - \hat{f}_{i-\frac{1}{2}}\right),
\end{cases} \tag{2.3}
$$

where $\bar{u}_i(t)$, $\bar{m}_i(t)$ and $\bar{p}_i(t)$ are the numerical approximation to the cell averages $\bar{u}(x_i,t)$, $\bar{m}(x_i,t)$ and $\bar{p}(x_i,t)$. The numerical fluxes $\hat{f}_{i+\frac{1}{2}}$, $\hat{m}_{i+\frac{1}{2}}$ and $\hat{p}_{i+\frac{1}{2}}$ are defined by

$$
\hat{f}_{i+\frac{1}{2}} = \hat{f}(u^-_{i+\frac{1}{2}}, u^+_{i+\frac{1}{2}}),\ \hat{m}_{i+\frac{1}{2}} = m^-_{i+\frac{1}{2}},\ \hat{p}_{i+\frac{1}{2}} = p^+_{i+\frac{1}{2}}. \tag{2.4}
$$

with $u^{\pm}_{i+\frac{1}{2}}$ obtained by the WENO reconstruction from the cell average $\bar{u}_i$, and $m^{\pm}_{i+\frac{1}{2}}, p^{\pm}_{i+\frac{1}{2}}$ obtained by the linear reconstruction from $\bar{m}_i, \bar{p}_i$. We choose the two arguments flux function $\hat{f}$ to be a monotone flux, which satisfies:

- $\hat{f}(a,b)$ is a Lipschitz continuous function in both arguments,
- $\hat{f}(a,b)$ is nondecreasing function in a and nonincreasing function in b.
- $\hat{f}(a,b)$ is consistent with the physical flux f, i.e. $\hat{f}(a,a) = f(a)$.

In our high order simulation, we use the less expensive local Lax-Friedrichs (LF) flux

$$
\hat{f}(a,b) = \frac{1}{2}(f(a) + f(b) - \alpha(b-a)), \tag{2.5}
$$

where $\alpha = \max_u |f'(u)|$ is a constant and the maximum is taken over the relevant range of u. And the numerical fluxes $\hat{m}$ and $\hat{p}$ are chosen from the opposite side of the cell interface point $x_{i+\frac{1}{2}}$, so called the alternating flux. The motivation of choosing these numerical fluxes comes from the total variation bounded (TVB) property of the equation. With the first order reconstruction (i.e. $u^-_{i+\frac{1}{2}} = \bar{u}_i, u^+_{i+\frac{1}{2}} = \bar{u}_{i+1}$) and the Euler forward time discretization, the TVB property can be proved for the first order fully discrete finite volume method (2.3) as the P^0 discontinuous Galerkin method for the DP equation in [26] and the first order finite difference method in [5].

In solving finite volume scheme (2.3), the reconstruction step can be described as the following. Given the cell averages $\{\bar{u}_i\}$, reconstruct a polynomial $q_i(x)$ for each cell I_i, such that it satisfies some accuracy and non-oscillatory property. In particular, this approximation gives the point values at the cell boundaries

$$
u^-_{i+\frac{1}{2}} := q_i(x_{i+\frac{1}{2}}),\ \ u^+_{i-\frac{1}{2}} := q_i(x_{i-\frac{1}{2}}).
$$

For first order schemes, the reconstruction is piecewise constant, while second order schemes can be obtained by a piecewise linear reconstruction. Higher order schemes are obtained by higher order polynomials. But for the piecewise smooth function $u(x)$, the oscillation happens when the stencil contains the discontinuous point (the discontinuous cell for cell averages). Thus, the accuracy is no longer valid. To avoid the discontinuous cell, essential non-oscillatory reconstruction (ENO) [11] was developed based on choosing the stencil adaptively. For k-th order accuracy, k candidate stencils are considered, covering $(2k-1)$ cells. The choosing strategy is based on the Newton form of the interpolation polynomial and comparing the Newton divided difference recursively. WENO reconstruction is based on ENO reconstruction, which combines all candidate stencils with nonlinear weights. Thus, it could achieve $(2k-1)$-th accuracy in smooth regions and choose a appropriate candidate stencil in non-smooth regions. The reader can consult the review by [21] and references therein for a more detailed description of high order non-oscillatory reconstructions.

In summary, the semi-discrete finite volume scheme can be proceeded as follows:

Finite volume WENO (FV-WENO) scheme

1. Given cell averages $\bar{u}$, use the WENO reconstruction to obtain $u^{\pm}_{i+\frac{1}{2}}$.
2. Form the scheme (2.3) with the monotone numerical flux $\hat{f}$, where the linear reconstruction is used for the numerical flux $\hat{m}$ and $\hat{p}$ in the elliptic problem.

For the time discretization method, we adopt the explicit TVD Runge-Kutta method [20], due to the total variation bounded property of the DP equation.

3. Finite difference method

In this section, we develop the finite difference WENO method for the DP equation based on the discrete L^2 stability property of the linear finite difference scheme.

3.1. Notation

The inner product and the associated norm of $L^2([-L,L])$ space are denoted by

$$(u,w) := \int_{-L}^{L} u(x)w(x)dx, \quad \|u\|_{L^2} = \sqrt{(u,u)}.$$

An important tool in the proof of L^2 norm stability of u is the quantity v, which has appeared in the energy E_2 of the DP equation. We can obtain the L^2 norm bound on the solution u in terms of the initial data u_0, by noticing that the following energy stability of v has been derived in [3]

$$\frac{d}{dt}\int_{-L}^{L}(2v^2+\frac{5}{2}v_x^2+\frac{1}{2}v_{xx}^2)dx=0, \tag{3.1}$$

where $4v - v_{xx} = u$. It follows that $u, v \in L^\infty(\mathbb{R}^+, L^2([-L, L]))$. And then we can get the L^2 stability of u that

$$\|u(x,t)\|_{L^2} \le 2\,\|u_0(x)\|_{L^2},$$

which is the key to develop the finite difference scheme.

In a finite difference scheme the basic unknown is the pointwise value of the function, rather than its cell average. Consider the grid function $u_h = \{u_j\}_{j=1}^N$ on the uniform grid $\{x_j\}_{j=1}^N$, where the grid interval is $h = 2L/N$. We define a discrete L^2 product and norm for grid functions by

$$(u_h, v_h)_h = h\sum_{j=1}^{N} u_j v_j \quad \text{and} \quad \|u_h\|_h^2 = (u_h, u_h)_h,$$

respectively.

We now denote the difference operator D as the approximation of the differential operators ∂_x. The conjugate operator D^* of D is defined as

$$(Du_h, v_h)_h = -(u_h, D^* v_h)_h.$$

For example, the first order forward difference operator D_+ is defined by

$$(D_+u_h)_j = (u_{j+1} - u_j)/h,$$

and its conjugate operator D_+^* is the backward difference operator D_-

$$(D_-u_h)_j = (u_j - u_{j-1})/h.$$

Another example is the central difference operator D_0,

$$(D_0u_h)_j = (u_{j+1} - u_{j-1})/2h,$$

which has the conjugate operator $D_0^* = D_0$.

Similarly, we define the differential operator Δ as the approximation of ∂_{xx}^2. The conjugate operator of Δ is denoted by Δ^*, where

$$(\Delta u_h, v_h)_h = (u_h, \Delta^* v_h)_h.$$

For the second order accurate approximation of ∂_{xx}^2, the central difference operator $\Delta = D_+ D_-$ has the conjugate operator $\Delta^* = \Delta$.

3.2. Linear finite difference scheme

The semi-discrete finite difference discretization for the DP equation (2.1) can be written as

$$\begin{cases} \partial_t u_h + \tilde{D} f(u_h) + p_h = 0, \\ p_h - \Delta p_h = 3\tilde{D} f(u_h), \end{cases} \tag{3.2}$$

where $f(u_h) = \{f(u_j)\}_{j=1}^N$ is the grid function. To obtain the L^2 stability, the operator $\tilde{D}$ is given by

$$\tilde{D} f(u_h) = \frac{2}{3} D f(u_h) + \frac{1}{3} u_h D^* u_h, \tag{3.3}$$

and Δ should have the property $\Delta^* = \Delta = DD^*$. Here, D and Δ could be any linear difference operators, e.g., $D = D_+$ and $\Delta = D_+ D_-$.

In order to prove the L^2 bound of the numerical solution u_h, we introduce the auxiliary grid function v_h, such that

$$4v_h - \Delta v_h = u_h. \tag{3.4}$$

Then we have the following energy stability relation lemma.

Lemma 3.1. *Assume $\Delta = DD^*$. Then*

$$\frac{d}{dt}\left\{2(v_h, v_h)_h + \frac{5}{2}(D^* v_h, D^* v_h)_h + \frac{1}{2}(\Delta v_h, \Delta v_h)_h\right\} = (\partial_t u_h, v_h - \Delta v_h)_h. \tag{3.5}$$

Proof. It follows by taking the time derivative of the equation (3.4), and taking discrete L^2 product with the grid function $v_h - \Delta v_h$. □

Next, we can prove the following energy conservation of v_h for the scheme (3.2).

Proposition 3.2. *In scheme (3.2), the following energy of v_h is conserved*

$$\frac{d}{dt}\left\{2(v_h, v_h)_h + \frac{5}{2}(D^* v_h, D^* v_h)_h + \frac{1}{2}(\Delta v_h, \Delta v_h)_h\right\} = 0. \tag{3.6}$$

Proof. In the scheme (3.2), by taking discrete L^2 product with $v_h - \Delta v_h$ and v_h for the first and second equations, we get

(3.7)
$$\begin{cases} (\partial_t u_h, v_h - \Delta v_h)_h + (\tilde{D} f(u_h), v_h - \Delta v_h)_h + (p_h, v_h - \Delta v_h)_h = 0, \\ (p_h - \Delta p_h, v_h)_h = (3\tilde{D} f(u_h), v_h)_h. \end{cases}$$

Since $\Delta^* = \Delta$, we find

$$(p_h - \Delta p_h, v_h)_h = (p_h, v_h - \Delta v_h)_h,$$

which implies that

$$(p_h, v_h - \Delta v_h)_h = (3\tilde{D} f(u_h), v_h)_h.$$

Substituting it into the first equation of (3.7), yields

$$(\partial_t u_h, v_h - \Delta v_h)_h + (\tilde{D} f(u_h), 4v_h - \Delta v_h)_h = 0.$$

Applying (3.4) and the lemma 2.1, gives

$$\frac{d}{dt}\left\{ 2(v_h, v_h)_h + \frac{5}{2}(D^* v_h, D^* v_h)_h + \frac{1}{2}(\Delta v_h, \Delta v_h)_h \right\} + (\tilde{D} f(u_h), u_h)_h = 0.$$

By the definition of $\tilde{D} f(u_h)$ in (3.3), we find

$$(\tilde{D} f(u_h), u_h)_h = 0.$$

Thus, we obtain the energy conservation of v_h. □

It follows from this proposition that we have the L^2 bound of the numerical solution u_h for the scheme (3.2).

Proposition 3.3. *For the finite difference scheme (3.2), the discrete L^2 norm of u_h is stable,*

$$\|u_h(\cdot, t)\|_h \leq 2 \|u_h(\cdot, 0)\|_h .$$

Proof. Using the auxiliary grid function v_h in (3.4), we find

$$\begin{aligned} (u_h, u_h)_h &= (4v_h - \Delta v_h, 4v_h - \Delta v_h)_h \\ &= 16(v_h, v_h)_h + 8(D^* v_h, D^* v_h)_h + (\Delta v_h, \Delta v_h)_h. \end{aligned}$$

It implies the following two inequalities,

$$(u_h, u_h)_h \le 8\left(2(v_h, v_h)_h + \frac{5}{2}(D^* v_h, D^* v_h)_h + \frac{1}{2}(\Delta v_h, \Delta v_h)_h\right),$$
$$(u_h, u_h)_h \ge 2\left(2(v_h, v_h)_h + \frac{5}{2}(D^* v_h, D^* v_h)_h + \frac{1}{2}(\Delta v_h, \Delta v_h)_h\right).$$

From the energy conservation of v_h in the proposition 3.2, we can derive

$$\begin{aligned}\|u_h(\cdot,t)\|_h^2 &\le 8\left(2(v_h, v_h)_h + \frac{5}{2}(D^* v_h, D^* v_h)_h + \frac{1}{2}(\Delta v_h, \Delta v_h)_h\right)(t)\\ &= 8\left(2(v_h, v_h)_h + \frac{5}{2}(D^* v_h, D^* v_h)_h + \frac{1}{2}(\Delta v_h, \Delta v_h)_h\right)(0)\\ &\le 4\,\|u_h(\cdot,0)\|_h^2.\end{aligned}$$

Thus, the discrete L^2 norm stability of u_h is obtained. □

3.3. Finite difference WENO scheme

To apply the WENO reconstruction in the finite difference scheme, we write the differential operator in conservation form

$$u_x = \frac{\hat{u}_{j+\frac{1}{2}} - \hat{u}_{j-\frac{1}{2}}}{h}, \tag{3.8}$$

where the flux $\hat{u}$ is defined by the sliding average operator

$$u(x) = \frac{1}{h}\int_{x-\frac{h}{2}}^{x+\frac{h}{2}} \hat{u}(\xi)d\xi. \tag{3.9}$$

Thus, $u(x_j)$ is the cell average of function $\hat{u}$ on the interval $[x_j - \frac{h}{2}, x_j + \frac{h}{2}]$. Therefore, $\hat{u}^{\pm}_{j+\frac{1}{2}}$ can be obtained by the same WENO reconstruction from the cell average of $\hat{u}$ on $[x_j - \frac{h}{2}, x_j + \frac{h}{2}]$ (i.e. $u(x_j)$) as in the finite volume method.

The difference operator $\tilde{D}$ in (3.3) can be written as

$$(\tilde{D} f(u_h))_j = \frac{2}{3}\frac{\hat{f}_{j+\frac{1}{2}} - \hat{f}_{j-\frac{1}{2}}}{h} + \frac{1}{3}u_j\frac{\hat{u}_{j+\frac{1}{2}} - \hat{u}_{j-\frac{1}{2}}}{h}, \tag{3.10}$$

The numerical fluxes $\hat{f}_{j+\frac{1}{2}}$ and $\hat{u}_{j+\frac{1}{2}}$ are obtained from WENO reconstruction for the discontinuous solution or linear reconstruction for smooth solution. To be consistent with the linear L^2 stable scheme, the following alternating numerical fluxes are used,

$$\hat{f}_{j+\frac{1}{2}} = \hat{f}^{-}_{j+\frac{1}{2}},\ \hat{u}_{j+\frac{1}{2}} = \hat{u}^{+}_{j+\frac{1}{2}},\ \text{or},\ \hat{f}_{j+\frac{1}{2}} = \hat{f}^{+}_{j+\frac{1}{2}},\ \hat{u}_{j+\frac{1}{2}} = \hat{u}^{-}_{j+\frac{1}{2}}. \tag{3.11}$$

In summary, the semi-discrete finite difference scheme can be proceeded as follows:

Finite difference WENO (FD-WENO) scheme

1. Given grid functions u_h and $f(u_h)$, use the WENO reconstruction to obtain $\hat{u}^{\pm}_{j+\frac{1}{2}}$ and $\hat{f}^{\pm}_{j+\frac{1}{2}}$.
2. Form the scheme (3.2) with the difference operator $\tilde{D}$ (3.10) of the alternating numerical fluxes (3.11). And the linear symmetric difference operator Δ is adopted for the elliptic problem.

By the method of lines, the TVD Runge-Kutta method [20] is used as in the finite volume method.

Remark 3.1. We can also develop the finite difference scheme based on the total variation bounded property. The difference operator $\tilde{D}$ is defined as

$$(\tilde{D}f(u_h))_j = \frac{\hat{f}_{j+\frac{1}{2}} - \hat{f}_{j-\frac{1}{2}}}{h}. \tag{3.12}$$

The numerical flux $\hat{f}_{j+\frac{1}{2}}$ is reconstructed with the smooth flux splitting

$$f(u) = f_p(u) + f_m(u),$$

where

$$\frac{df_p(u)}{du} \geq 0,\ \frac{df_m(u)}{du} \leq 0.$$

From the grid functions $f_p(u_h)$ and $f_m(u_h)$, we use the WENO reconstruction to obtain $\hat{f}^{-}_{p,j+\frac{1}{2}}$ and $\hat{f}^{+}_{m,j+\frac{1}{2}}$ separately. Then the numerical flux is given by

$$\hat{f}_{j+\frac{1}{2}} = \hat{f}^{-}_{p,j+\frac{1}{2}} + \hat{f}^{+}_{m,j+\frac{1}{2}}.$$

The less expensive Lax-Friedrichs splitting can be adopted

$$f_p(u) = f(u) + \alpha u,\ \ f_m(u) = f(u) - \alpha u,$$

where α is taken as $\alpha = \max_u |f'(u)|$ over the relevant range of u as the Lax-Friedrichs flux used in the finite volume method. Similarly, the TVB

property can be proved for the first order reconstruction and Euler forward time discretization [5].

4. Numerical examples

In this section we provide numerical examples to illustrate the accuracy and capability of the proposed algorithms. For the time discretization method, we adopt the explicit TVD Runge-Kutta method [20], due to the total variation bounded property of the DP equation. Even with the third order spatial derivative in the equation, the time step for both schemes is $\Delta t \approx h$, because the inverse operator of $I - \partial_{xx}$ is applied at each time step. For the problems without the analytic solutions, the numerical results are shown to be numerically convergent, with the aid of successive mesh refinement. These numerical simulation mainly comes from [24, 26] for easy comparison.

Example 4.1. Accuracy test for smooth soliton solutions

Consider the traveling wave solution $u(x,t) = U(x-ct)$ of the DP equation, where c is the wave speed. Let $\xi = x - ct$, and assume $\lim_{\xi\to\infty} U(\xi) = A$. The smooth soliton solutions have been constructed explicitly in [28]. When we set $A = 1$ and $c = 5$, an explicit formula of the smooth soliton solution can be obtained as

$$U(\xi) = A((4-\sqrt{5}) - \frac{2\sqrt{5}}{X(\xi)^2 - 1}),$$

where $X(\xi)$ is defined by

$$\begin{aligned} X(\xi) = (&-\frac{7+3\sqrt{5}}{3}b + \frac{38+17\sqrt{5}}{27}b^3 \\ &+ \sqrt{\frac{2+\sqrt{5}}{27} + \frac{517+231\sqrt{5}}{54}b^2 - \frac{521+233\sqrt{5}}{54}b^4})^{\frac{1}{3}} \\ &+ (-\frac{7+3\sqrt{5}}{3}b + \frac{38+17\sqrt{5}}{27}b^3 \\ &- \sqrt{\frac{2+\sqrt{5}}{27} + \frac{517+231\sqrt{5}}{54}b^2 - \frac{521+233\sqrt{5}}{54}b^4})^{\frac{1}{3}} \\ &+ \frac{2+\sqrt{5}}{3}b, \end{aligned}$$

with $b = \frac{1+e^{|\xi|}}{1-e^{|\xi|}}$. We use the finite difference and finite volume schemes separately with the fifth order WENO reconstruction. The L^2 and L^∞ errors and

Table 1: Accuracy test for smooth soliton solutions in Example 4.1: L^2 and L^∞ errors of u, at time $t = 1$ in the domain $[-50, 50]$

	FD-WENO				FV-WENO			
N	L^2 error	order	L^∞ error	order	L^2 error	order	L^∞ error	order
160	2.70E-03	–	1.55E-03	–	3.70E-03	–	2.28E-03	–
320	1.20E-04	4.49	8.24E-05	4.24	1.52E-04	4.60	9.82E-05	4.53
640	3.80E-06	4.98	2.58E-06	5.00	4.68E-06	5.02	3.10E-06	4.99
1280	1.19E-07	5.00	8.09E-08	5.00	1.43E-07	5.03	9.65E-08	5.00
2560	3.60E-09	5.04	2.46E-09	5.04	4.31E-09	5.05	2.93E-09	5.04

the numerical orders of accuracy are contained in Table 1, at time $t = 1$ in the domain $[-50, 50]$. We set the time step small enough so that the spatial discretization error is dominated in the simulation. From the table, it shows that both schemes can achieve the designed fifth order accuracy.

In the following simulations, the finite volume and finite difference WENO schemes perform very similarly. So we only show the numerical results from the FD-WENO scheme with the fifth order WENO reconstruction for simplicity.

Example 4.2. Single peakon and anti-peakon traveling solutions

In this example, we present the traveling waves of peakon and anti-peakon solutions $u(x,t) = ce^{-|x-ct|}$, and $u(x,t) = -ce^{-|x+ct|}$. The peakon and anti-peakon solutions do not have enough regularity, so the DP equation is satisfied in the distribution sense. We choose the traveling speed $c = 1$ and the computational domain $[-40, 40]$ with $N = 640$. In Figs. 1 and 2, the peakon and anti-peakon profiles are shown at times $t = 4, 8, 12$ and 16 with the exact solutions. These traveling waves are smooth everywhere except the wave crest. We can see that the moving peakon and anti-peakon are well resolved.

Example 4.3. Two-peakons interaction and two-anti-peakons interaction:

In this example, we consider the two-peakons interaction of the DP equation with the initial condition

$$u = c_1 e^{-|x-x_1|} + c_2 e^{-|x-x_2|}.$$

where the parameters $c_1 = 2, c_2 = 1, x_1 = -13.792$ and $x_2 = -4$. The same parameters are used in the two-anti-peakons interaction, with the initial condition

$$u = -c_1 e^{-|x+x_1|} - c_2 e^{-|x+x_2|}.$$

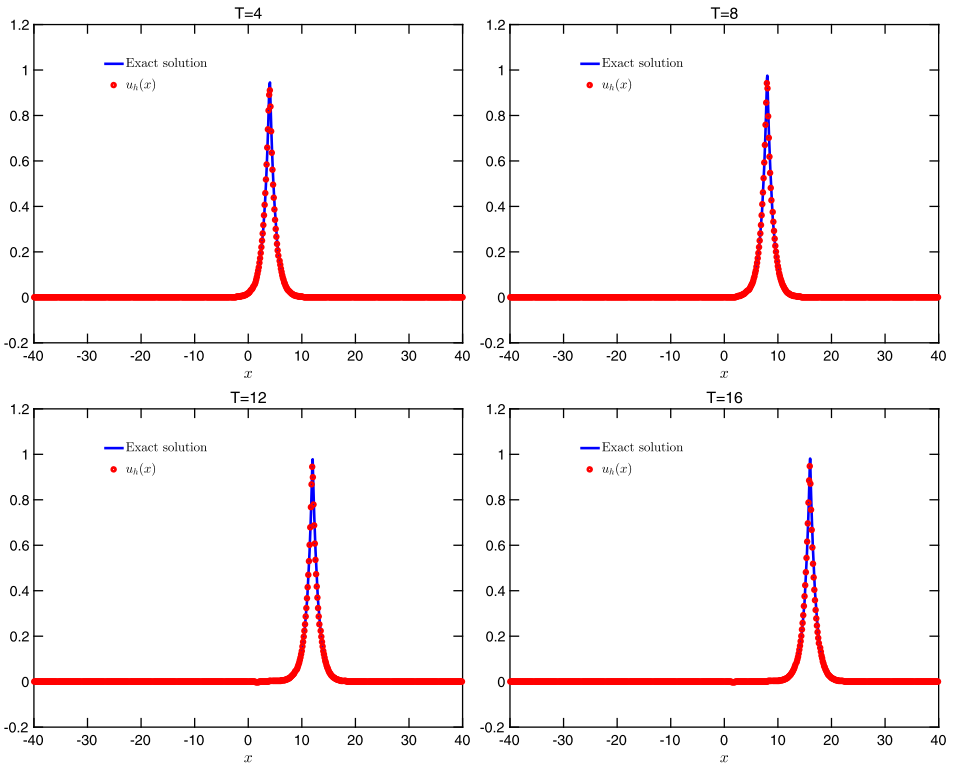

Figure 1: Numerical results of the peakon solitons at different times $t = 4, 8, 12$ and 16 with $N = 640$ in the domain $[-40, 40]$, comparing with the exact solution.

In these interactions, the soliton should preserve its shape and velocity before and after encountering a nonlinear interaction with other similar soliton. In Figs. 3 and 4, the interactions profiles show at times $t = 0, 4, 8$ and 12 in the domain $[-40, 40]$ with $N = 640$. We can see that the moving peakons interactions are resolved very well. And numerically it shows that these interactions are elastic processes.

Example 4.4. Shock peakon solution

The DP equation also admits shock peakon solution

$$u(x,t) = -\frac{1}{t+1}\text{sign}(x)e^{-|x|},$$

which contains a discontinuity at $x = 0$. The presence of shock peakon solutions means that the DP equation admits solution that is less regular

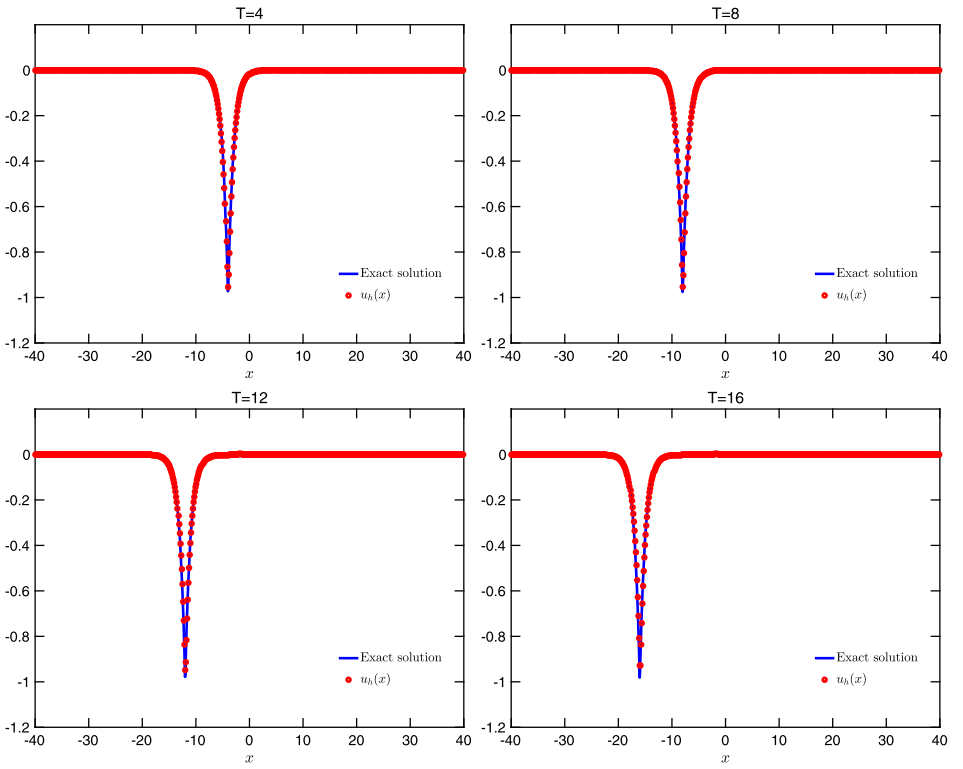

Figure 2: Numerical results of the anti-peakon solitons at different times $t = 4, 8, 12$ and 16 with $N = 640$ in the domain $[-40, 40]$, comparing with the exact solution.

than the CH equation, which makes the difference between the DP and CH equations. In this example, the simulation is performed in the domain $[-25, 25]$ with $N = 640$. Because of the shock discontinuity in the solution, the numerical oscillations could appear for the linear schemes. In the Fig. 5, the numerical results u_h have been showed comparing with the exact solution. We can see that the solution can be resolved without spurious oscillations due to the WENO reconstruction.

Example 4.5. Peakon and anti-peakon interaction

For the DP equation, the shock can also be formed between the peakon and anti-peakon interaction, with the initial condition

$$u(x, 0) = c_1 e^{-|x-x_1|} - c_2 e^{-|x-x_2|};$$

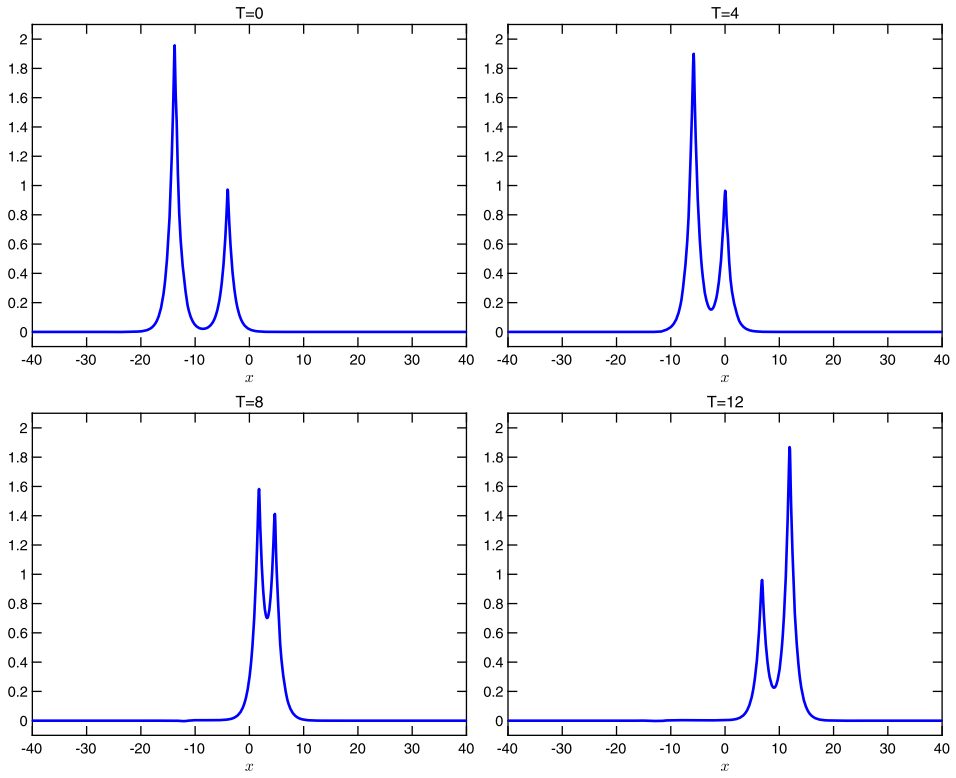

Figure 3: Numerical results of two-peakon interaction at different times $t = 0, 4, 8$ and 12 with $N = 640$ in the domain $[-40, 40]$.

where $c_1 = 1, c_2 = 1, x_1 = -5$ and $x_2 = 5$. In the CH equation, the peakon and anti-peakon will pass through each other after the collision. But the DP equation will generate shocks in the collision. Fig. 6 shows the numerical solution u_h with $N = 640$ in the domain $[-20, 20]$. Similarly, and the shock is fully resolved in the numerical result with the help of WENO reconstruction.

Example 4.6. Triple interaction

In this example, we consider the interaction among peakon, anti-peakon and one stationary shock peakon of the DP equation, with the initial condition

$$u(x, 0) = e^{-|x+5|} + \text{sign}(x)e^{-|x|} - e^{-|x-5|}.$$

The computational domain is $[-20, 20]$. Fig. 7 shows the numerical results at time $t = 7$ with $N = 256$. From the figure, it shows that there are two shocks

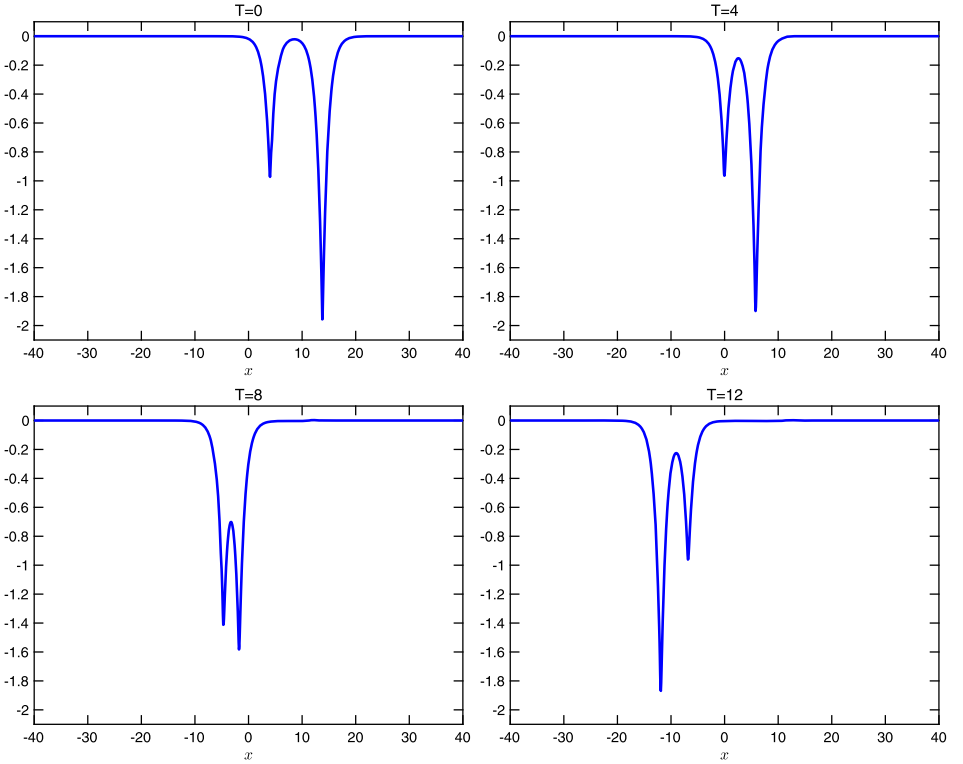

Figure 4: Numerical results of anti-two-peakon interaction at different times $t = 0, 4, 8$ and 12 with $N = 640$ in the domain $[-40, 40]$.

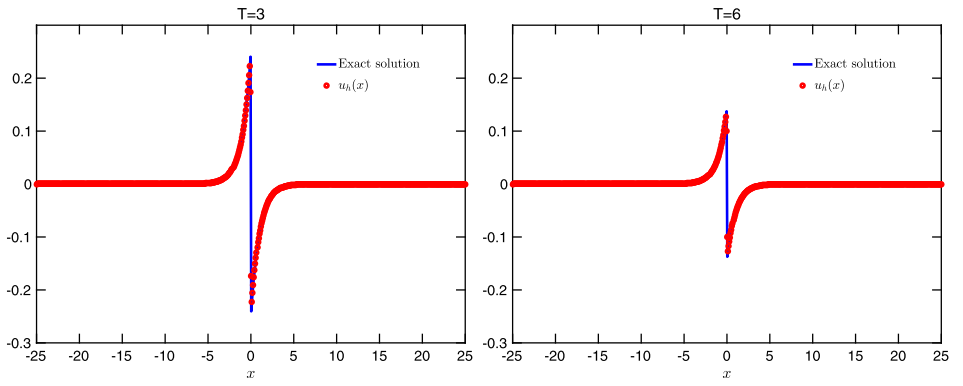

Figure 5: Numerical results of shock peakon solution at time $t = 3, 6$ with $N = 640$ in the domain $[-25, 25]$, comparing with the exact solution.

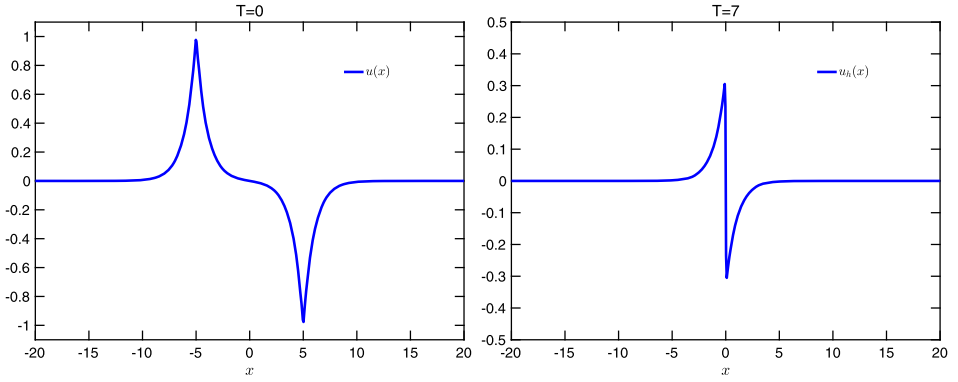

Figure 6: Numerical results of shock peakon solution at time $t = 0, 7$ with $N = 640$ in the domain $[-20, 20]$.

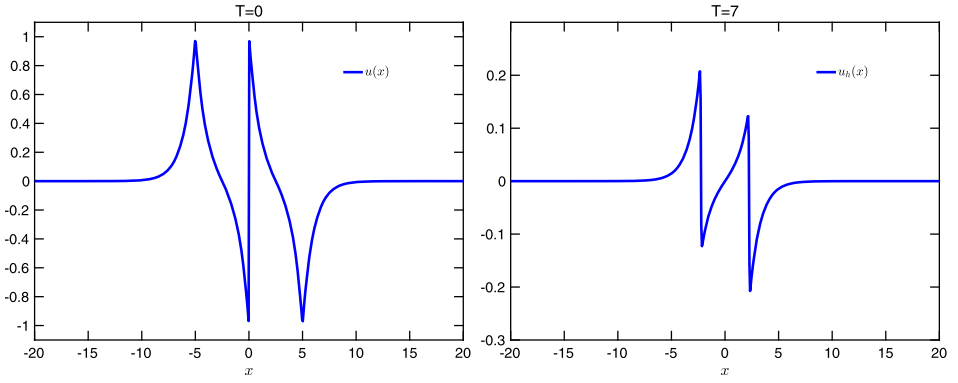

Figure 7: Numerical results of the interaction among peakon, anti-peakon and one stationary shock peakon, at time $t = 0, 7$ with $N = 640$ in the domain $[-20, 20]$.

formed at this time. It is showed that the solution with multiple shocks are resolved very well by the finite difference WENO scheme.

Example 4.7. Shock formation

In this example, we consider the shock formation with the smooth initial condition:

$$u(x, 0) = e^{0.5x^2} \sin(\pi x).$$

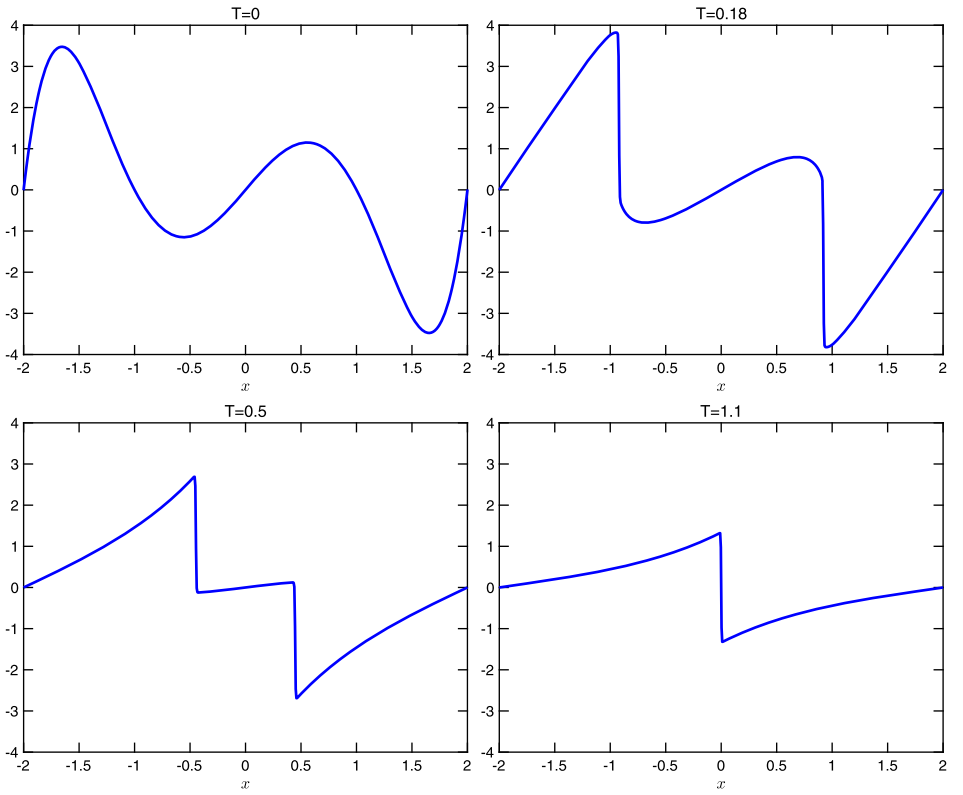

Figure 8: Numerical results of shock formation at time $t = 0, 0.18, 0.5, 1.1$ with $N = 640$, in the domain $[-2, 2]$.

Fig. 8 shows the numerical results u_h at time $t = 0.18, 0.5, 1.1$ with $N = 640$ in the domain $[-2, 2]$. We can see that even with the smooth initial condition shock appears in finite time. These numerical tests show that the finite difference method coupled with the WENO reconstruction can resolve the solution of the DP equation very well, with or without the discontinuity.

5. Conclusion

We developed the weighted essentially non-oscillatory (WENO) finite volume and finite difference schemes for the DP equation, based on the total variation bounded property and L^2 stability property separately. The DP equation are prone to develop discontinuous solutions in finite time even with smooth initial condition. The WENO reconstruction is adopted in both

schemes to resolve the peakon and shock solutions successfully. Comparing with the DG method in [26] or the spectral method in [24], the finite volume and finite difference WENO methods can also achieve high order accuracy for the smooth solutions, but no limiter or post-processing procedure is needed for the discontinuous solutions. Numerical examples are given to show the accuracy and the capacity of these methods.

References

[1] D.S. Balsara, and C.-W. Shu, Monotonicity preserving weighted essentially non-oscillatory schemes with increasingly high order of accuracy. J. Comput. Phys. **160**, 405–452 (2000). MR1763821

[2] W. Cai, Y. Sun, and Y. Wang, Geometric numerical integration for peakon b-family equations. Commun. Comput. Phys. **19**, 24–52 (2016). MR3448693

[3] G.M. Coclite, and K.H. Karlsen, On the well-posedness of the Degasperis-Procesi equation. J. Funct. Anal. **233**, 60–91 (2006). MR2204675

[4] G.M. Coclite, and K.H. Karlsen, On the uniqueness of discontinuous solutions to the Degasperis-Procesi equation. J. Differ. Equ. **234**, 142–160 (2007). MR2298968

[5] G.M. Coclite, K.H. Karlsen, and N.H. Risebro, Numerical schemes for computing discontinuous solutions of the Degasperis-Procesi equation. IMA J. Numer. Anal. **28**(1), 80–105 (2008). MR2387906

[6] A. Constantin, and D. Lannes, The hydrodynamical relevance of the Camassa-Holm and Degasperis-Procesi equations. Arch. Rat. Mech. Anal. **192**, 165–186 (2009). MR2481064

[7] A. Degasperis, and M. Procesi, Asymptotic integrability. In: Degasperis, A., Gaeta, G. (eds.) Symmetry and Perturbation Theory, pp. 23–37. World Scientific Publishers, River Edge, NJ (1999). MR1844104

[8] A. Degasperis, D.D. Holm, and A. Hone, A new integrable equation with peakon solutions. Theor. Math. Phys. **133**, 1463–1474 (2002). MR2001531

[9] H.R. Dullin, G.A. Gottwald, and D.D. Holm, On asymptotically equivalent shallow water wave equations. Phys. D **190**, 1–14 (2004). MR2043789

[10] B. Feng, and Y. Liu, An operator splitting method for the Degasperis-Procesi equation. J. Comput. Phys. **228**, 7805–7820 (2009). MR2561844

[11] A. Harten, B. Engquist, S. Osher, and S. Chakravarthy, Uniformly high order essentially non-oscillatory schemes, III. J. Comput. Phys. **71**, 231–303 (1987). MR0897244

[12] H. Hoel, A numerical scheme using multi-shockpeakons to compute solutions of the Degasperis-Procesi equation. Electron. J. Differ. Equ. **2007**, 1–22 (2007). MR2328701

[13] R. Ivanov, Water waves and integrability. Philos. Trans. R. Soc. A **365**, 2267–2280 (2007). MR2329147

[14] G.-S. Jiang, and C.-W. Shu, Efficient implementation of weighted ENO schemes. J. Comput. Phys. **126**, 202–228 (1996). MR1391627

[15] R.S. Johnson, The classical problem of water waves: a reservoir of integrable and nearly-integrable equations. J. Nonlinear Math. Phys. **10**(Supplement 1), 72–92 (2003). MR2063546

[16] H. Liu, Y. Huang, and N. Yi, A Conservative discontinuous Galerkin method for the Degasperis-Procesi equation. Methods Appl. Anal. **21**, 67–89 (2014). MR3257960

[17] X. Liu, S. Osher, and T. Chan, Weighted essentially non-oscillatory schemes. J. Comput. Phys. **115**, 200–212 (1994). MR1300340

[18] H. Lundmark, Formation and dynamics of shock waves in the Degasperis-Procesi equation. J. Nonlinear Sci. **17**, 169–198 (2007). MR2314847

[19] Y. Miyatake, and T. Matsuo, Conservative finite difference schemes for the Degasperis-Procesi equation. J. Comput. Appl. Math. **236**, 3728–3740 (2012). MR2923506

[20] C.-W. Shu, and S. Osher, Efficient implementation of essentially non-oscillatory shock capturing schemes. J. Comput. Phys. **77**, 439–471 (1988). MR0954915

[21] C.-W. Shu, Essentially non oscillatory and weighted essentially non-oscillatory schemes for hyperbolic conservation laws. In: Advanced numerical approximation of nonlinear hyperbolic equations, Lecture Notes in Mathematics, **1697**, 325–432 (2000). MR1728856

[22] C.-W. Shu, High order weighted essentially non-oscillatory schemes for convection dominated problems. SIAM Rev. **51**, 82–126 (2009). MR2481112

[23] C.-W. Shu, High order WENO and DG methods for time-dependent convection-dominated PDEs: a brief survey of several recent developments. J. Comput. Phys. **316**, 598–613 (2016). MR3494371

[24] Y. Xia, Fourier spectral methods for Degasperis-Procesi equation with discontinuous solutions. J. Sci. Comput. **61**, 584–603 (2014). MR3268661

[25] Y. Xu, and C.-W. Shu, A local discontinuous Galerkin method for the Camassa-Holm equation. SIAM J. Numer. Anal. **46**, 1998–2021 (2008). MR2399405

[26] Y. Xu, and C.-W. Shu, Local discontinuous Galerkin methods for the Degasperis-Procesi equation. Commun. Comput. Phys. **10**, 474–508 (2011). MR2799652

[27] C.H. Yu, and T.W.H. Sheu, A dispersively accurate compact finite difference method for the Degasperis-Procesi equation. J. Comput. Phys. **236**, 493–512 (2013). MR3020068

[28] G. Zhang, and Z. Qiao, Cuspons and smooth solitons of the Degasperis-Procesi equation under inhomogeneous boundary condition. Math. Phys. Anal. Geom. **10**, 205–225 (2007). MR2368959

Yinhua Xia
School of Mathematical Sciences
University of Science and Technology of China
Hefei, Anhui 230026
P.R. China
E-mail address: yhxia@ustc.edu.cn

Yan Xu
School of Mathematical Sciences
University of Science and Technology of China
Hefei, Anhui 230026
P.R. China
E-mail address: yxu@ustc.edu.cn

Received June 27, 2016